Progress in Natural Science: Materials International 2012;22(4):273–280

Chinese Materials Research Society

Progress in Natural Science: Materials International

www.elsevier.com/locate/pnsmi
www.sciencedirect.com

ORIGINAL RESEARCH

Synthesis and characterization of conducting polyaniline nanocomposites containing ZnO nanorods

Amir Mostafaei[a,*], **Ashkan Zolriasatein**[b]

[a]*Faculty of Materials Engineering, Sahand University of Technology, Tabriz, Iran*
[b]*Advanced Materials and Nanotechnology Research Laboratory, Faculty of Mechanical Engineering, K.N. Toosi University of Technology, Tehran, Iran*

Received 30 March 2012; accepted 4 June 2012
Available online 14 August 2012

KEYWORDS

Conductive polymer;
Polyaniline based nanocomposite;
ZnO nanorods;
Chemical synthesis

Abstract Polyaniline (PANI) based nanocomposites filled with ZnO nanorods were prepared by the chemical oxidative method of the aniline in acid medium with ammonium peroxydisulphate (APS) as an oxidant. The composition, morphology and structure of the polymer and the nanocomposites were characterized by Fourier transform infrared spectroscopy (FTIR), X-ray diffraction (XRD), transmission electron microscopy (TEM), scanning electron microscopy (SEM), thermogravimetric analysis (TGA), UV–vis spectroscopy and electrical conductivity. The characteristic FTIR peaks of PANI were found to shift to higher or lower wave number in PANI–ZnO composites due to formation of H-bonding. Different amounts of ZnO nanorods were used to verify this effect on the characteristics of the synthesized materials. These observed effects have been attributed to interaction of ZnO nanorods with PANI molecular chains. XRD results revealed that the crystallinity of PANI was more pronounced after addition of nanorods, while the intensity of the peaks increased by addition of ZnO nanorods. Electrical conductivity of the PANI–ZnO nanocomposite film was found to be smaller than that of the PANI film. The decrease of electrical conductivity in PANI–ZnO films as compared to PANI was attributed to the interfaces formed between oxygen of ZnO nanorods and hydrogen of PANI. Also, TGA results showed that the decomposition of the nanocomposite was less than that of pure polyaniline which confirms the successful fabrication of products. These conductive polymers can be used in commercial paints as an additive.

*Correspondence to: No. 12, Firouzeh Alley, Hajipour street, Resalat Avenue, Tehran 16318-13573, Iran. Tel.: +98 21 22505214.
E-mail address: amir.mostafaei@gmail.com (A. Mostafaei).

Peer review under responsibility of Chinese Materials Research Society.

Production and hosting by Elsevier

1. Introduction

In recent years, developments of inorganic–organic hybrid materials on nanometer scale have been receiving significant attention due to a wide range of potential applications and high absorption in the visible part of the spectrum and high mobility of the charge carriers. Polyaniline is the most attractive

http://dx.doi.org/10.1016/j.pnsc.2012.07.002

conductive polymer because of the presence of the reactive –NH– groups in polymer chain [1–3], and used in broad applications such as batteries [4], sensors [5,6], electronic devices [7], supercapacitors [8] and corrosion protection in organic coatings [9–11] due to its physical and chemical properties, good electrical conductivity (p-type), high environmental stability, low cost [12,13], light weight, flexibility, facile fabrication and possibility of both chemical and electrochemical syntheses [14–16]. Electrical conductivity of polyaniline is a very important parameter and it could be modified by the addition of inorganic fillers [17]. Additionally, electrical conductivity of polyaniline depends on dopant ions [18–20].

Metals and semiconducting nanostructure materials are used as stabilizers or capping agents of these conducting polymers. In recent decades, several reports have been published on the synthesis of the PANI nanocomposites with the inorganic nano-scale such as TiO_2 [21–23], CdS [7], Silica [24], Ag [25,26], Na^+-montmorillonite [13,27], CeO_2 [28], Fe_3O_4 [5,29], Zn [9] and MnO_2 [12]. These nanocomposites exhibit many new characters, such as electrical, optical, catalytic and mechanical properties that the single material does not have. Nowadays, nano-scale semiconducting materials such as TiO_2 and ZnO with n-type conductivity [1] and UV-sensitivity are added in a conductive organic matrix for combination of electrical conductivity and UV-sensitivity. Most recently, PANI–TiO_2 composites were synthesized and studied as well [4,21–23], but about PANI–ZnO nanocomposites specially filled with nanorods morphology, there is less attention. ZnO is a semiconducting material that has direct wide band gap (3.37 eV) and large excition binding energy (60 meV) at room temperature [20,30]. Zinc oxide (ZnO) is a nontoxic material, n-type semiconductor with a good photocatalytic activity [31]. The structure and morphology of ZnO have an important effect on its properties and applications; thus, several parameters such as reaction time, rate of evaporation and precursor concentration are found to determine the growth of ZnO nanostructures like nanoparticles, nanorods and nanospheres. The one dimensional nanostructure such as nanorod, nanowire and nanotube has obtained more attention in various applications due to its potential as a building block for other structures especially in paints and coatings. Furthermore, its electrical and optical properties are better due to the reduced carrier scattering in one dimensional structure [32,33]. This one dimensional nanostructure has gained enormous attention due to its extraordinary characteristics in photonics, optics and electronics, and therefore has been used in various industries such as rubber, medical and dental, pigments and coatings, catalysts, ceramic, concrete and in chemical synthesis [31,34,35].

In this paper, PANI and its nanocomposites with ZnO nanorods were fabricated by in situ oxidative polymerization of aniline monomer with ammonium peroxydisulphate (APS). The products were characterized by FTIR spectra (FTIR), X-ray diffraction (XRD), electron microscopy (TEM, SEM), thermogravimetric analysis (TGA), UV–vis spectroscopy and electrical conductivity. The interaction between PANI and ZnO nanorods was investigated and the results demonstrate doping effect of ZnO nanorods. The aim of the production of PANI–ZnO nanocomposite is applying it as an additive in marine paint for improving anticorrosive and antifouling properties.

2. Experimental

2.1. Chemical and instrumentations

ZnO nanorods were synthesized according to the method proposed by Wu et al. [36]. The results of the phase and structural characterization of ZnO nanorods by XRD [35–37] and TEM are presented in Figs. 1 and 2, respectively. The TEM analysis of ZnO nanorods (Fig. 2), reveals that ZnO nanorods have diameters ranging between 20 and 50 nm and lengths ranging between 50 and 200 nm. Commercially available aniline (Fluka, Purity 99.5%) was distilled under reduced pressure. Tetraethylenpentamine (TEPA, Merck purity 99%) was used as received without any purification. Ammonium peroxydisulfate (APS, Merck) and camphorsulfonic acid (CSA, Merck) were used as an oxidant and acid dopant,

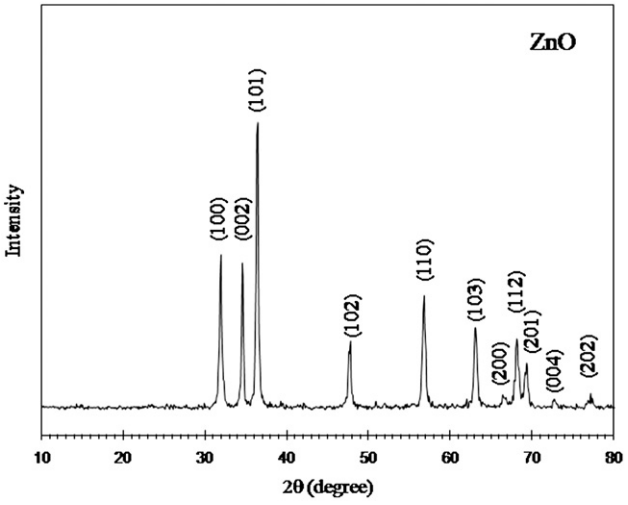

Fig. 1 XRD pattern of ZnO nanorods.

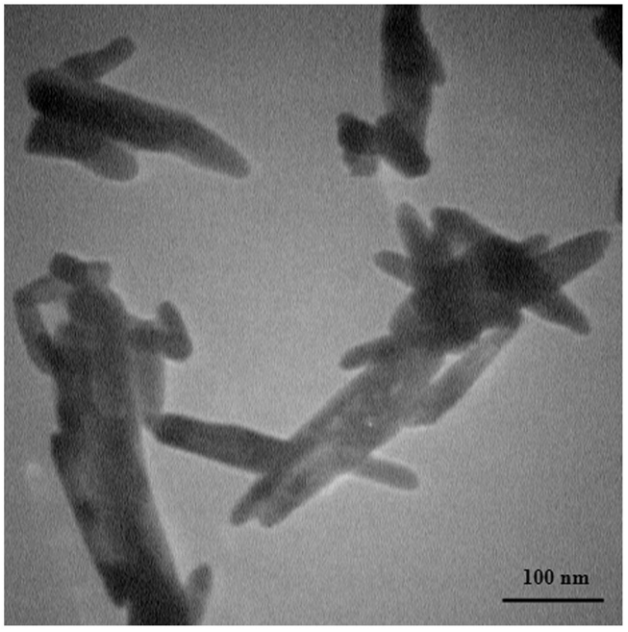

Fig. 2 TEM micrograph of ZnO nanorods.

respectively. All aqueous solutions were prepared with distilled water. Then, the synthesized composites were characterized by the following methods:

(i) *FTIR spectroscopy*—Fourier transform infrared (FT-IR) spectra were recorded with a Bruker Tensor 27 spectrometer over the wave number range of 4000–400 cm^{-1}. The spectra of ZnO nanorods, PANI and PANI–ZnO nanocomposites were taken using KBr disks.

(ii) *XRD analysis*—The powder X-ray diffraction (XRD) patterns were recorded on a D8 Advance-Bruckers AXS diffractometer with Cu-Kα radiation source ($\lambda = 1.54$Å) operated at 40 kV and 40 mA in the 2θ range 10–80° at the scan speed of 0.05° per second.

(iii) *Electron microscopy analysis*—The transmission and scanning electron micrographs of PANI and nanocomposites were analyzed using a SEM Oxford (Model TeScan) and TEM (Ziess 100 kV), respectively; the pigment was spread over an aluminum block over which gold was sputtered in order to prepare for SEM studies.

(iv) *TG analysis*—Thermogravimetric analysis (TGA) was carried out using an STA 1500 instrument at a heating rate of 10 °C min^{-1} in N_2.

(v) *UV–vis spectroscopy*: UV–vis spectra were recorded on a T80+/PG Instruments Ltd spectrophotometer in the range of 320–1100 nm.

(vi) *Electrical conductivity*—The electrical conductivities of PANI and nanocomposites were found by a four probe resistivity meter at room temperature.

2.2. Preparation of PANI

A series of CSA-doped polyaniline (PANI) latex was synthesized via in situ emulsion polymerization. A typical procedure to prepare the CSA-doped PANI is given as follows: 0.003 mol (0.704 g) of CSA was mixed with 0.05 mol (4.5 g) of aniline monomer in 200 mL of distilled water for 2 h. The mixture was pre-cooled to ~0 °C in an ice bath, to form a homogeneous dispersion of aniline–CSA complex. Then, 50 mL of aqueous solution containing 0.04 mol (9 g) of APS was added dropwise into the emulsion while stirring at 0 °C temperature. After ~4 h, the precipitate was collected on a Buchner funnel and repeatedly rinsed with water. The products were then dried in an oven for 12 h. The green color of all the four samples obtained was the first evidence of the polyaniline formation in its conductive form, emeraldine salt (ES).

2.3. Preparation of PANI–ZnO nanocomposite

To prepare PANI–ZnO composites of different ratios, the following steps were followed. 0.045, 0.090 and 0.180 g of ZnO nanorods were mixed with 0.05 mol (4.5 g) of aniline monomer in 200 mL of distilled water in a set of reaction vessels. The mixtures were stirred with magnetic stirrers in ice water baths for 4 h to get a uniform suspension of the composite. The work-up procedure was the same as described in previous section. From these reactions, pure PANI and PANI–ZnO nanocomposites with compositions given in Table 1 were achieved.

3. Results and discussions

3.1. FTIR spectroscopy

PANI and PANI–ZnO nanocomposites were characterized by using the FTIR technique. Fig. 3 shows the FTIR pattern of ZnO nanorods, PANI and PANI–ZnO nanocomposites and characteristic absorption peaks are given in Table 2. The characteristic absorption bands of PANI are 515.71 cm^{-1} (C–N–C bonding mode of aromatic ring), 592.85 cm^{-1} and 700.84 cm^{-1} (C–C, C–H bonding mode of aromatic ring), 831.98 cm^{-1} (C–H out of plane bonding in benzenoid ring), 1040.26 $cm^{-1}$and 1155.97 cm^{-1} (S=O bonding for camphursulfonic acid), 1302.53 $cm^{-1}$and 1503.09 cm^{-1} (C–N stretching of benzenoid ring) and 1572.52 cm^{-1} (C=N stretching of quinoid ring). The PANI–ZnO nanocomposites show the same characteristic peaks. However, there is an evidence of peak displacement when ZnO nanorods are added to the PANI. These shifts include 1572.51–1587.94 cm^{-1}, 1503.09–1510.81 cm^{-1}, 1155.97–1148.25 cm^{-1}, 1040.26–1047.97 cm^{-1}, 831.98–862.84 cm^{-1}, and 592.85–600.23 cm^{-1}. Furthermore, in PANI–ZnO nanocomposites, a broad peak appeared in 3470 cm^{-1} which can be associated to the interaction between ZnO nanorods and PANI by formation of hydrogen bonding between H–N and oxygen of ZnO, so the peak displacement which was observed in FTIR spectra may be ascribed to the formation of hydrogen bonding between ZnO and the N–H group of PANI on the surface of the ZnO nanorods [38,39] which influence the electron densities of the PANI chain. For instance, C–N, C–N and C=C bonds are shifted to the higher wavenumbers which are stronger in nanocomposites while N–H is shifted to the lower one which is weakened. According to the patterns, absorption intensity is increased by adding ZnO nanorods in the case of nanocomposites due to uniform distribution of ZnO nanorods in nanocomposites matrix and elimination of agglomeration.

3.2. XRD analysis

XRD analysis was used to examine the structure of the PANI and PANI–ZnO nanocomposites and investigate the effect of the various amounts of ZnO nanorods on the PANI structure. Fig. 4

Table 1 Quantity of pure materials used and content of ZnO nanorods in nanocomposite.

Sample	Aniline (g)	Nano-ZnO (g)	ZnO in aniline (%)	Nanocomposite yield (g)	ZnO in product (%)[a]
PANI	4.5	–	–	3.227	0
PANI–ZnO 1 wt%	4.5	0.045	1	3.392	1.327
PANI–ZnO 2 wt%	4.5	0.090	2	3.468	2.595
PANI–ZnO 4 wt%	4.5	0.180	4	3.635	4.952

[a](g ZnO/g composite) × 100.

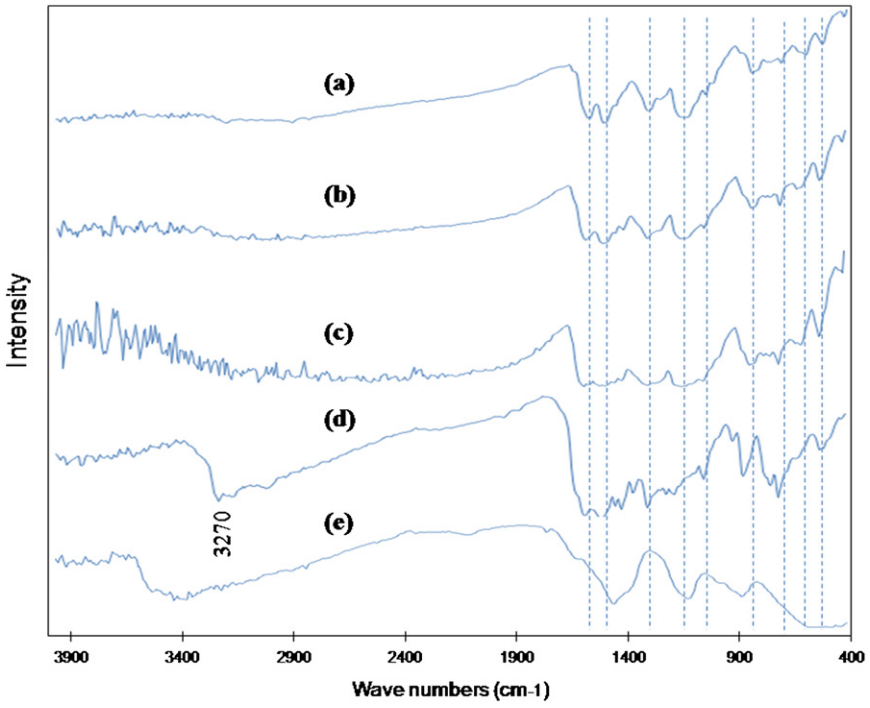

Fig. 3 FTIR pattern of (a) PANI, (b)–(d) PANI–ZnO 1 wt%, 2 wt% and 4 wt% nanocomposites and (e) ZnO nanorods.

Table 2 Characteristic absorption peaks obtained from FTIR spectrum of ZnO nanorods, PANI and PANI–ZnO nanocomposite.

Wavenumber (cm^{-1})	functionality
515–595	C–N–C bonding mode of aromatic ring
650–750	C–C, C–H bonding mode of aromatic ring
830–860	C–H out of plane bonding in benzenoid ring
1040–1155	S═O bonding for camphursulfonic acid
1230–1310	C–N stretching of benzenoid ring
1503–1511	C–N stretching of benzenoid ring
1570–1595	C═N Stretching of quinoid ring
2800–3000	Symmetric stretch vibration band of methylene [–$(CH_2)_n$–] and methyl –(CH_3)
3270	Interaction between ZnO and PANI by formation of hydrogen bonding between H–N and oxygen of ZnO
3500–4000	Vibration band of –OH

shows the typical XRD patterns of PANI and PANI–ZnO nanocomposites. As is evident in PANI and its nanocomposites, broad diffraction peaks occur between 10° and 30° due to the parallel and perpendicular periodicity of the polymer (PANI) chain. The PANI peak diffracted at an angle of $2\theta = 19.31°$ and $2\theta = 25.72°$ with a d spacing 4.593 Å and 3.461 Å, respectively, in the XRD pattern which shows low crystallinity of the conductive polymers due to the repetition of benzenoid and quinoid rings in PANI chains [23]; moreover, PANI crystal size, D, is 4.4 nm which was calculated by Scherrer's equation [29]. In the presence of ZnO nanorods, crystal size of nanocomposites increased from 4.4 nm for PANI to 5.3 nm, 5.5 nm and 8.2 nm for PANI–ZnO 1 wt%., 2 wt% and 4 wt% nanocomposite, respectively. It can be seen that the XRD patterns of nanocomposites are similar to that of PANI. This is because of the negligible content of ZnO nanorods which is less than 5% and it has no effect on diffraction pattern of PANI. According to Fig. 4, in the given range recorded for the broad peak, two distinct sharp peaks at $2\theta = 19.31°$ and $2\theta = 25.72°$ with planes of (010) and (200), respectively, are shifted negligibly but their intensity increases as the content of ZnO nanorods in PANI–ZnO nanocomposite increased. Additionally, one peak at $2\theta = 23.2°$ with plane of (102) appears which is related to PANI–CSA and its intensity is increased by adding ZnO nanorods. XRD results confirm previous results' test which depict the effect of ZnO nanorods in PANI–ZnO nanocomposites. As expected, low percentage of ZnO nanorods have no effect on the identity of PANI while they can make progress in properties of this conductive polymer. Fig. 4 shows that intensity of the peaks was increased by increasing amount of ZnO nanorods which means that there is an interaction of ZnO nanorods and PANI by formation of hydrogen bonding between H–N and oxygen of ZnO [23].

3.3. *SEM and TEM studies*

Morphologies of the PANI and PANI–ZnO nanocomposite with different ZnO nanorods contents are shown in Fig. 5. All the nanocomposites reveal flaky shaped structure, in which the

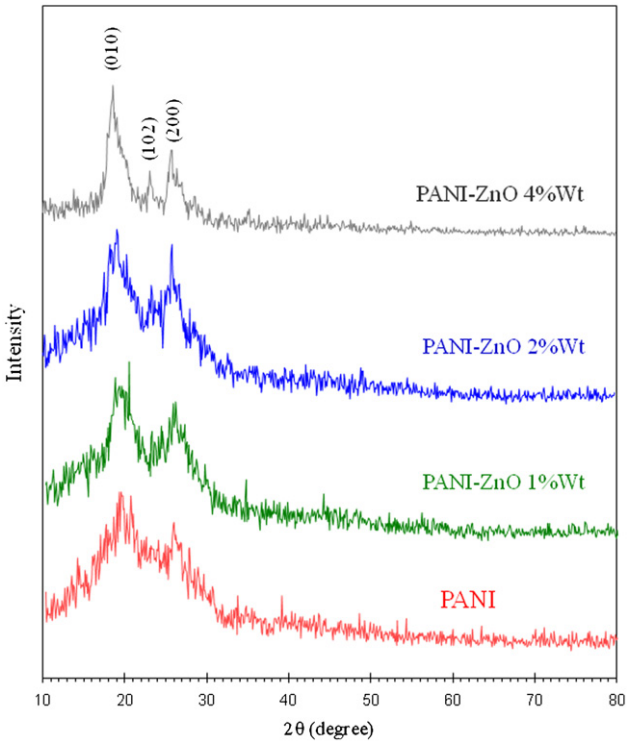

Fig. 4 X-Ray pattern of PANI and PANI–ZnO nanocomposites.

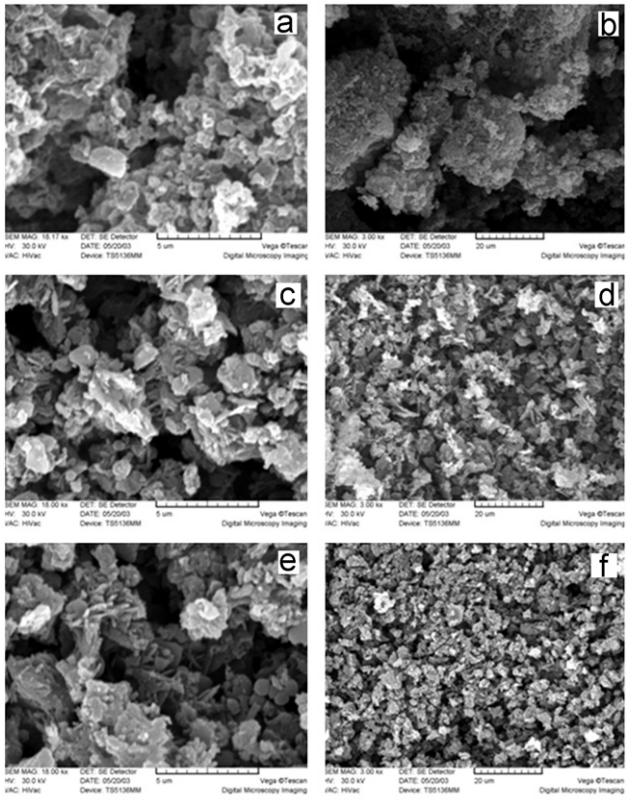

Fig. 5 Scanning electron micrograph of (a, b) PANI–ZnO 1 wt%, (c, d) PANI–ZnO 2 wt% and (e, f) PANI–ZnO 4 wt% nanocomposites.

size of flakes reduces as more percentage of ZnO nanorods is added into PANI. It can be seen that the size of final crystals of ZnO covered by PANI reduced with increasing ZnO nanorods content due to the possibility of agglomeration of ZnO particles, and PANI has declined. These nanocomposites should give the opportunity to obtain improved capacitance due to surface effects. The SEM images help us draw a conclusion that the doping of ZnO nanorods has a strong effect on the morphology of PANI, since PANI has various structure such as granules, nanofibers, nanotubes, nanospheres, microspheres and flakes [3].

Due to the low magnification in SEM micrographs, it is difficult to observe ZnO nanorods in the nanocomposite matrix, thus an appropriate way for observing them in polymer matrix nanocomposite is the use of TEM. According to the TEM micrographs in Fig. 6, PANI and ZnO nanorods have formed a nanocomposite in which the nanorods are embedded in the polymer matrix. It is obvious that ZnO nanorods were uniformly coated by PANI.

3.4. *TG analysis*

The thermogravimetric (TGA) analysis of camphor-doped polyaniline under heating rate of 10 °C min^{-1} is shown in Fig. 7. The results reveal that the trend of PANI–ZnO nanocomposite degradation is similar to PANI. It can be seen that the thermal degradation of PANI occurs at 275 °C and the initial mass loss at lower temperature is mainly due to release of either water (up to 125 °C) or dopant anions (275 °C). Also, the weight loss occurring around 240 °C is due to the removal of dopants and the weight loss occurring right after 350 °C corresponds to the decomposition of the polymer. In the TGA curve of ZnO nanorods, weight loss is about 2.5% which is due to the adsorbed water and moisture. In PANI–ZnO nanocomposites, decomposition is reduced because of a strong interaction at the interface of ZnO and PANI [23,39], which supports our claim that the presence of ZnO nanorods can improve properties of the conductive polymer. Finally, after decomposition and degradation of materials, total residues of 36.34% (wt%) for PANI and 59.15%, 60.13% and 62.67% (wt.%) for PANI–ZnO nanocomposites (1 wt%, 2 wt%, and 4 wt% ZnO nanorods) were obtained.

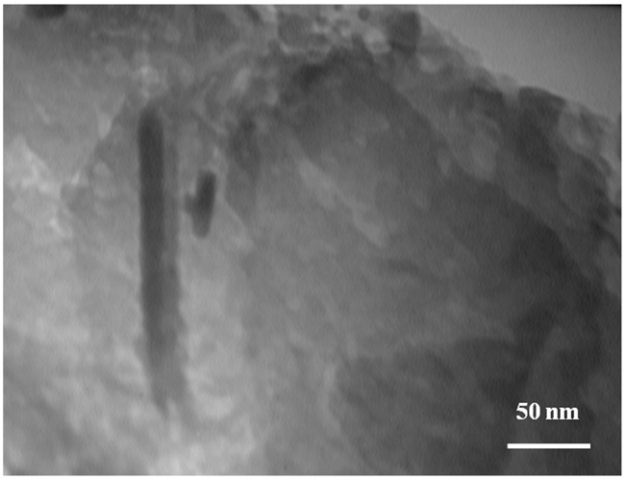

Fig. 6 TEM micrograph of PANI–ZnO 2 wt% nanocomposite.

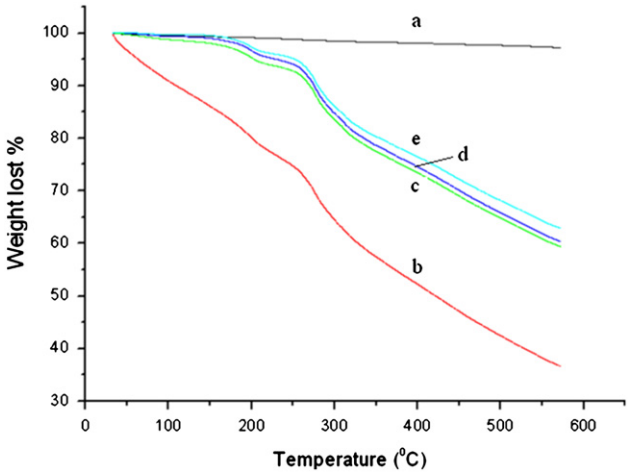

Fig. 7 TGA curves of (a) ZnO nanorods, (b) PANI, (c) PANI–ZnO 1 wt%, (d) PANI–ZnO 2 wt% and (e) PANI–ZnO 4 wt% nanocomposites.

Table 3 Electrical conductivity of PANI, ZnO nanorods and PANI–ZnO nanocomposites.

Electrical conductivity (S cm^{-1})	Composition
0.016	Nano-ZnO
0.025	PANI–CSA
0.0068	PANI–ZnO 1 wt%
0.0029	PANI–ZnO 2 wt%
0.0014	PANI–ZnO 4 wt%

3.5. *Electrical conductivity*

Electrical conductivities of ZnO, PANI and PANI–ZnO nanocomposites is described in Table 3. The range of electrical conductivity of PANI is widespread from 10^{-10} to 10^{3} S/cm based on the acid dopant and fillers [20,40]. Electrical conductivities of PANI and ZnO nanorods are 0.025 S/cm and 0.016 S/cm, respectively, while in PANI–ZnO 1 wt.%nanocomposite, electrical conductivity is around 0.0068 S/cm. Results show that electrical conductivity of PANI decayed on adding ZnO. This can be attributed to adsorption of –NH of PANI on the surface of ZnO nanorods and bond formation in the structure. In addition, the decrease of conductivity of PANI–ZnO nanocomposites may be ascribed to the behavior of ZnO in the nanocomposites or reduction of doping degree [5]. As mentioned, the conductivity of the polymer depends on the nature of dopant and the inorganic materials concentration, which have an important role in conductivity of the nanocomposites [21–23,28,29]. Additionally, rising amount of ZnO nanorods from 1 wt%to 2 wt% and 4 wt% influenced on electrical conductivity and decreased from 0.0068 to 0.0029 and 0.0014 S/cm. The reason is that with increasing amount of ZnO nanorods, the possibility of bond formation between –NH of PANI on the surface of ZnO nanorods is increased and the relative contents of the conducting polymer (PANI) decreased [21]. Furthermore, these results support other spectroscopy's results such as TGA, XRD and FTIR data where they prove the theory of bond formation between PANI and ZnO nanorods.

3.6. *UV–vis spectroscopy*

In order to investigate optical properties of fabricated materials, UV–vis spectroscopy was carried out on products. The UV–vis spectrum of PANI and PANI–ZnO nanocomposites are shown in Fig. 8. PANI has two characterization absorption bands at around 336 nm and 628 nm that attributed to π–π* transition of the benzenoid ring and n–π* transition of benzenoid to quinoid, respectively [5,26]. It has been found that the shapes of UV spectra of nanocomposites are similar to those of PANI and some shifting in the bands is noticed. In the case of PANI–ZnO 1 wt%, 2 wt% and 4 wt% nanocomposites, the peak around 615–628 nm is ascribed to the selective interaction between ZnO and quinoid ring of polyaniline (ES). Furthermore, by addition of ZnO nanorods, intensity of the peak around 615–628 nm increased due to interaction between ZnO nanorods and PANI molecules and wavelength decreased due to the interaction between oxygen in ZnO nanorods and –NH in PANI. Additionally, the peak of PANI around 336 nm is based on the π–π* transition of the benzenoid ring where the peaks of PANI–ZnO

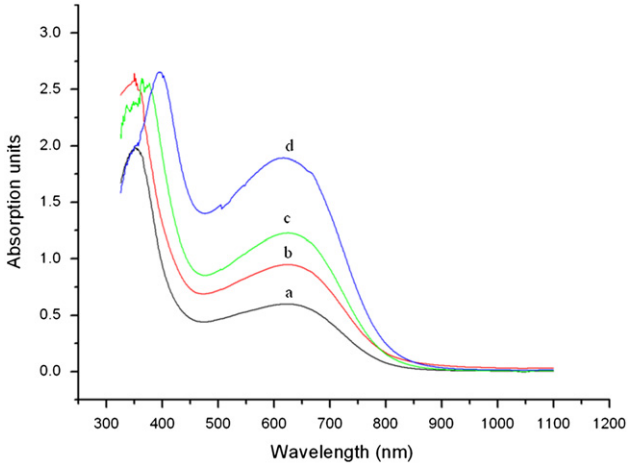

Fig. 8 UV–vis spectra of (a) PANI, (b) PANI–ZnO 1 wt% nanocomposite, (c) PANI–ZnO 2 wt% nanocomposite and (d) PANI–ZnO 4 wt% nanocomposite.

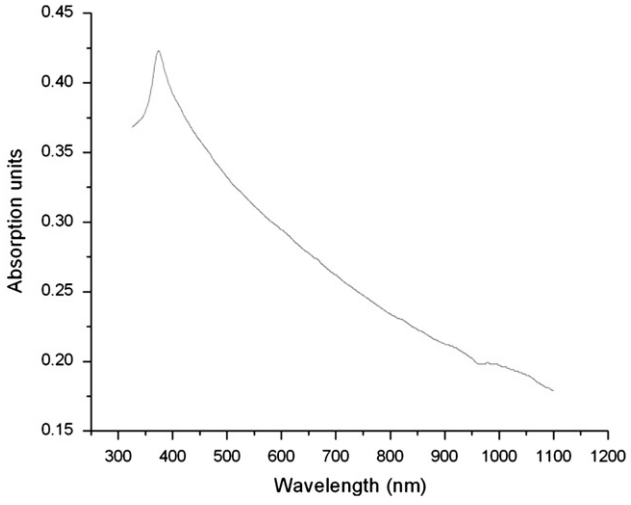

Fig. 9 UV–vis spectrum of ZnO nanorods.

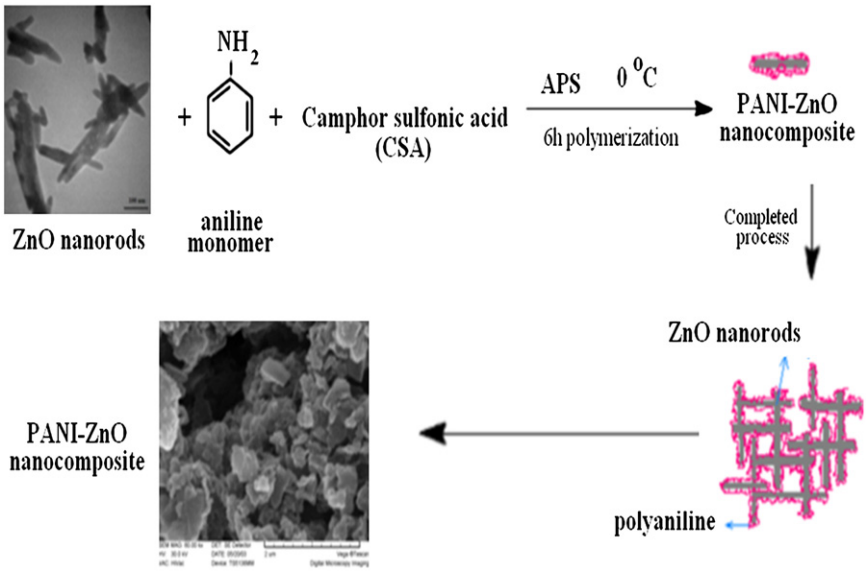

Fig. 10 Schematic diagram of the formation of polyaniline–ZnO nanocomposite.

nanocomposites 1 wt%, 2 wt%and 4 wt% were around 350, 377 and 396 nm, respectively, which shows redshifts. Fig. 9 shows UV–vis spectroscopy of ZnO nanorods. In Fig. 9 there is a broad band at 374 nm which is the characteristic band of pure ZnO nanorods [1], while the characteristic peak of ZnO nanorods cannot be detected in PANI–ZnO nanocomposites due to presence of low amount of ZnO nanorods in fabricated materials. This result is in a good agreement with X-ray diffraction patterns of these nanocomposites.

3.7. *Formation mechanism of PANI–ZnO nanocomposite*

A feasible mechanism for the formation of the PANI–ZnO nanocomposites is shown in Fig. 10. When aniline, APS, CSA, ZnO nanorods and water were mixed and stirred with magnetic stirrers, the Pickering emulsion of oil-in-water type was formed. Due to the rich hydroxyl groups existing on the surface of the nanorods, the water wettability of ZnO nanorods was stronger than their oil wettability. The CSA solution of aniline was in the droplets, while the water solution of APS became the continuous phase. The ZnO nanorods spontaneously assembled at the surfaces of CSA droplets, forming CSA/ZnO structures. Aniline in the droplets diffused to the CSA/water interface, adsorbed at the surface of the ZnO nanorods and polymerized under the oxidation of APS to yield PANI. PANI covered the ZnO nanorods, forming PANI–ZnO nanocomposites. An oxidant (APS) is added to induce the polymerization of aniline and the aniline molecules are polymerized around the surface of ZnO nanorods. With the proceeding of the polymerization reaction, the components of the solid shells were changed from the initial pure ZnO nanorods to the PANI–ZnO nanocomposites.

4. Conclusion

A series of ZnO doped polyaniline nanocomposites have been prepared by in situ chemical oxidative polymerization at atmospheric pressure and under visible light. The results of spectroscopic methods such as XRD, FTIR, TEM, SEM, TGA, electrical conductivity and UV–vis measurements indicate that PANI–ZnO nanocomposite is successfully prepared in this research.

A possible mechanism for the formation of the PANI–ZnO nanocomposites was proposed. XRD and FTIR results show that interaction between ZnO and PANI is based on the formation of hydrogen bonding and electrostatic interaction between camphorsulfonic acid capped ZnO nanorods and polyaniline plays a key role in the formation of the PANI–ZnO nanocomposite. Electrical conductivity measurements demonstrate that the conductivity of nanocomposites is less than those of PANI and ZnO nanorods and by increasing ZnO nanorods content, value of electrical conductivity decreased. SEM and TEM micrograph shows that there is a uniform distribution of ZnO nanorods in PANI-ZnO nanocomposite. Furthermore, TGA and UV–vis results confirm that –NH– group was adsorbed on the surface of ZnO nanorods as the thermal and optical properties have been changed. Further research on these nanocomposites in marine paints as an anticorrosive and antifouling additives is in progress.

Acknowledgments

The authors would like to express their thanks to Mr. Arjang Tajbakhsh (Faculty of Applied Science and Engineering, University of Toronto, Toronto, Canada) for his careful reading and comments on this manuscript. Also, we appreciate the support of the Iran Nanotechnology Initiative Council (INIC). We would like to acknowledge the Faculty of Materials Engineering in Sahand University of Technology and Department of Physical Chemistry of Tabriz University.

References

[1] S. Ameen, M.S. Akhtar, S.G. Ansari, O. Yang, H.S. Shin, Electrophoretically deposited polyaniline/ZnO nanoparticles for p–n heterostructure diodes, Superlattices and Microstructures 46 (2009) 872–880.

[2] S. Sathiyanarayanan, S.S. Azim, G. Venkatachari, Preparation of polyaniline–TiO_2 composite and its comparative corrosion protection performance with polyaniline, Synthetic Metals 157 (2007) 205–213.
[3] J. Stejskal, I. Sapurina, M. Trchová, Polyaniline nanostructures and the role of aniline oligomers in their formation, Progress In Polymer Science 35 (2010) 1420–1481.
[4] K. Gurunathan, D.P. Amalnerkar, D.C. Trivedi, Synthesis and characterization of conducting polymer composite (PAn/TiO_2) for cathode material in rechargeable battery, Materials Letters 57 (2003) 1642–1648.
[5] J. Deng, C.L. He, Y. Peng, J. Wang, X. Long, P. Li, A.S.C. Chan, Magnetic and conductive Fe_3O_4–polyaniline nanoparticles with core–shell structure, Synthetic Metals 139 (2003) 295–301.
[6] N.G. Deshpande, Y.G. Gudage, R. Sharma, J.C. Vyas, J.B. Kim, Y.P. Lee, Studies on tin oxide-intercalated polyaniline nanocomposite for ammonia gas sensing applications, Sensors and Actuators B: Chemical 138 (2009) 76–84.
[7] W. Jia, E. Segal, D. Kornemandel, Y. Lamhot, M. Narkis, A. Siegmann, Polyaniline-DBSA/organophilic clay nanocomposites: synthesis and characterization, Synthetic Metals 128 (2002) 115–120.
[8] C. Peng, S. Zhang, D. Jewell, G.Z. Chen, Carbon nanotube and conducting polymer composites for supercapacitors, Progress In Natural Science 18 (2008) 777–788.
[9] A. Olad, M. Barati, H. Shirmohammadi, Conductivity and anticorrosion performance of polyaniline/zinc composites: investigation of zinc particle size and distribution effect, Progress in Organic Coatings 72 (2011) 599–604.
[10] S. Sathiyanarayanan, V. Karpakam, K. Kamaraj, S. Muthukrishnan, G. Venkatachari, Sulphonate doped polyaniline containing coatings for corrosion protection of iron, Surface and Coatings Technology 204 (2010) 1426–1431.
[11] M. Behzadnasab, S.M. Mirabedini, K. Kabiri, S. Jamali, Corrosion performance of epoxy coatings containing silane treated ZrO_2 nanoparticles on mild steel in 3.5% NaCl solution, Corrosion Science 53 (2011) 89–98.
[12] X. Zhang, L. Ji, S. Zhang, W. Yang, Synthesis of a novel polyaniline-intercalated layered manganese oxide nanocomposite as electrode material for electrochemical capacitor, Journal of Power Sources 173 (2007) 1017–1023.
[13] B.H. Kim, J.H. Jung, S.H. Hong, J.W. Kim, H.J. Choi, J. Joo, Physical characterization of emulsion intercalated polyaniline–clay nanocomposite, Current Applied Physics 1 (2001) 112–115.
[14] G.K. Prasad, T. Takei, Y. Yonesaki, N. Kumada, N. Kinomura, Hybrid nanocomposite based on $NbWO_6$ nanosheets and polyaniline, Materials Letters 60 (2006) 3727–3730.
[15] B.K. Sharma, A.K. Gupta, N. Kharea, S.K. Dhawan, H.C. Gupta, Synthesis and characterization of polyaniline–ZnO composite and its dielectric behavior, Synthetic Metals 159 (2009) 391–395.
[16] R.C. Patil, S. Radhakrishnan, Conducting polymer based hybrid nano-composites for enhanced corrosion protective coatings, Progress in Organic Coatings 57 (2006) 332–336.
[17] L. Li, J. Jiang, F. Xu, Synthesis and ferrimagnetic properties of novel Sm-substituted LiNi ferrite–polyaniline nanocomposite, Materials Letters 61 (2007) 1091–1096.
[18] M.M. Ayad, E.A. Zaki, Doping of polyaniline films with organic sulfonic acids in aqueous media and the effect of water on these doped films, European Polymer Journal 44 (2008) 3741–3747.
[19] S.F. Chung, T.C. Wen, A. Gopalan, Influence of dopant size on the junction properties of polyaniline, Materials Science and Engineering B 116 (2005) 125–130.
[20] Y. Long, Z. Chen, N. Wang, J. Li, M. Wan, Electronic transport in PANI-CSA/PANI-DBSA polyblends, Physica B: Condensed Matter 344 (2004) 82–87.
[21] J.C. Xu, W.M. Liu, H.L. Li, Titanium dioxide doped polyaniline, Materials Science and Engineering C 25 (2005) 444–447.
[22] T.C. Mo, H.W. Wang, S.Y. Chen, Y.C. Yeh, Synthesis and dielectric properties of polyaniline/titanium dioxide nanocomposites, Ceramics International 34 (2008) 1767–1771.
[23] L. Shi, X. Wang, L. Lu, X. Yang, X. Wu, Preparation of TiO_2/polyaniline nanocomposite from a lyotropic liquid crystalline solution, Synthetic Metals 159 (2009) 2525–2529.
[24] P. Liu, Preparation and characterization of conducting polyaniline/silica nanosheet composites, Current Opinion in Solid State and Materials Science 12 (2008) 9–13.
[25] S. Jing, S. Xing, L. Yu, Y. Wu, C. Zhao, Synthesis and characterization of Ag/polyaniline core–shell nanocomposites based on silver nanoparticles colloid, Materials Letters 61 (2007) 2794–2797.
[26] P.K. Khanna, N. Singh, S. Charan, A.K. Visawanath, Synthesis of Ag/polyaniline nanocomposite via an in situ photoredox mechanism, Materials Chemistry and Physics 92 (2005) 214–219.
[27] B.H. Kim, J.H. Jung, J.W. Kim, H.J. Choi, J. Joo, Physical characterization of polyaniline–Na^+–montmorillonite nanocomposite intercalated by emulsion polymerization, Synthetic Metals 117 (2001) 115–118.
[28] Y. He, Synthesis of polyaniline/nano-CeO_2 composite microspheres via a solid-stabilized emulsion route, Materials Chemistry and Physics 92 (2005) 134–137.
[29] W. Xue, K. Fang, H. Qiu, J. Li, W. Mao, Electrical and magnetic properties of the Fe_3O_4–polyaniline nanocomposite pellets containing DBSA-doped polyaniline and HCl-doped polyaniline with Fe_3O_4 nanoparticles, Synthetic Metals 156 (2006) 506–509.
[30] R.-q. CHEN, C.-w. ZOU, X.-d. YAN, W. GAO, Zinc oxide nanostructures and porous films produced by oxidation of zinc precursors in wet-oxygen atmosphere, Progress in Natural Science: Materials International 21 (2011) 81–96.
[31] A. Moezzi, A.M. McDonagh, M.B. Cortie, Zinc oxide particles: synthesis, properties and applications, Chemical Engineering Journal 185–186 (2012) 1–22.
[32] S. Anitha, B. Brabu, D.J. Thiruvadigal, C. Gopalakrishnan, T.S. Natarajan, Optical, bactericidal and water repellent properties of electrospun nano-composite membranes of cellulose acetate and ZnO, Carbohydrate Polymers 87 (2012) 1065–1072.
[33] P. Amornpitoksuk, S. Suwanboon, S. Sangkanu, A. Sukhoom, N. Muensit, Morphology, photocatalytic and antibacterial activities of radial spherical ZnO nanorods controlled with a diblock copolymer, Superlattices and Microstructures 51 (2012) 103–113.
[34] M.-D.J. Schmidt-Mende L, ZnO—nanostructures, defects, and devices, Materials Today 10 (2007) 40–48.
[35] X.-Y. Ma, W.-D. Zhang, Effects of flower-like ZnO nanowhiskers on the mechanical, thermal and antibacterial properties of waterborne polyurethane, Polymer Degradation and Stability 94 (2009) 1103–1109.
[36] C. Wu, X. Qiao, J. Chen, H. Wang, F. Tan, S. Li, A novel chemical route to prepare ZnO nanoparticles, Materials Letters 60 (2006) 1828–1832.
[37] B. Kulyk, V. Kapustianyk, V. Tsybulskyy, O. Krupka, B. Sahraoui, Optical properties of ZnO/PMMA nanocomposite films, Journal of Alloys and Compounds 502 (2010) 24–27.
[38] B.K. Sharma, N. Khare, S.K. Dhawan, H.C. Gupta, Dielectric properties of nano ZnO-polyaniline composite in the microwave frequency range, Journal of Alloys and Compounds 477 (2009) 370–373.
[39] H. He, Preparation of polyaniline/nano-ZnO composites via a novel Pickering emulsion route, Powder Technology 147 (2004) 59–63.
[40] I.S. Lee, J.Y. Lee, J.H. Sung, H.J. Choi, Synthesis and electrorheological characteristics of polyaniline–titanium dioxide hybrid suspension, Synthetic Metals 152 (2005) 173–176.